AGU100 ADVANCING EARTH AND SPACE SCIENCE

Geophysical Research Letters

RESEARCH LETTER

10.1029/2018GL077555

Key Points:

- The 25-km-long Hess Deep rift is the transitional segment from rifting to seafloor spreading at the western tip of the Cocos-Nazca Rift
- The intrarift ridge, located within Hess Deep, is interpreted as an active, long-lived detachment fault
- Intrarift ridge formation may be in response to the slowdown in spreading rate associated with the development of the Galapagos microplate

Correspondence to:
D. K. Smith,
dksmith@nsf.gov

Citation:
Smith, D. K., & Schouten, H. (2018). Opening of Hess Deep Rift at the Galapagos Triple Junction. *Geophysical Research Letters*, *45*, 3942–3950. https://doi.org/10.1029/2018GL077555

Received 28 JUN 2015
Accepted 13 APR 2018
Accepted article online 24 APR 2018
Published online 8 MAY 2018

Opening of Hess Deep Rift at the Galapagos Triple Junction

Deborah K. Smith[1] **and Hans Schouten**[2]

[1]National Science Foundation, Alexandria, VA, USA, [2]Department of Geology and Geophysics, Woods Hole Oceanographic Institution, Woods Hole, MA, USA

Abstract At the Galapagos triple junction, the westward propagating Cocos-Nazca (C-N) Rift breaks into ~0.5 Ma crust accreted at the East Pacific Rise. Rifting transitions to full magmatic seafloor spreading in the wake of the propagating tip. The 25-km-long Hess Deep rift is the transitional segment from rifting to spreading. Intrarift ridge (IRR), located within Hess Deep rift, is interpreted as a detachment fault, which exhumes deep-seated rocks to the seafloor. Although transitional segments must have occurred throughout the westward propagation of C-N Rift, IRR is the only obvious detachment fault along the base of the Rift scarps in the last ~5 Ma of its propagation. IRR formation may be in response to a decrease in spreading rate (~40 to <20 mm/yr) and presumed lower melt supply, resulting from the formation of the Galapagos microplate ~1.4 Ma, which now controls the opening at the C-N Rift tip.

Plain Language Summary At the Galapagos triple junction in the equatorial Pacific three mid-ocean ridges come together: North East Pacific Rise (EPR), South EPR, and Cocos-Nazca (C-N) Rift. The C-N Rift, however, stops short of intersecting the EPR. The tip of the C-N Rift propagates westward toward the EPR, breaking apart ~0.5-million-year-old crust built at the EPR. Rifting of the crust changes to full magmatic seafloor spreading in the wake of the propagating C-N Rift tip, and the segment that is transitional from rifting to spreading has been identified. The intrarift ridge (IRR) is located within the transitional segment. IRR is interpreted as a long-ived fault, which has brought deep-seated rocks to the seafloor. The IRR is the only long-lived fault identified in the last ~5-million years of C-N Rift propagation implying that a long-lived fault is not a common stage in the transition to spreading. The IRR fault may be a result of the slowdown in spreading rate, and presumed decrease in the amount of magma rising beneath the segment, caused by the formation of the Galapagos microplate ~ 1.4-million years ago.

1. Introduction

In the past few decades, there have been many studies to understand the transition from rifting of the lithosphere to the establishment of seafloor spreading (e.g., Bonatti, 1985; Lonsdale, 1989; Manighetti et al., 1997; Taylor et al., 1995; Van Wijk & Blackman, 2005). Most studies have examined this transition where continental lithosphere is being rifted apart (e.g., Almalki et al., 2015, and references therein; Augustin et al., 2014; Bonatti, 1985; Hayward & Ebinger, 1996; Ligi et al., 2012; Martinez & Cochran, 1988; Rosendahl, 1987; Taylor et al., 1999, 1995; Van Wijk & Blackman, 2005). It has been argued that deformation starts in rheologically weak zones, and as the lithosphere is stretched and thinned, magma supply is established (e.g., Taylor et al., 1999). It has also been argued that magma upwelling dictates where rifting begins (e.g., Bastow et al., 2010; Hayward & Ebinger, 1996; Ligi et al., 2012). As of now, there is no consensus on the relative contributions of magmatism and faulting as seafloor spreading is established.

In this paper, we investigate the initiation of seafloor spreading at the Galapagos triple junction where the westernmost tip of the Cocos-Nazca (C-N) Rift (Figure 1) breaks apart ~0.5 Ma oceanic crust accreted on the East Pacific Rise (EPR) near 2°15′N (Lonsdale, 1988). The morphology of the rift segments developing in the wake of the Rift tip indicates that Hess Deep rift is the segment where the transition from rifting to full magmatic spreading takes place. Based on the observed style of faulting, we speculate on the relative importance of faulting and magmatism along this transition segment.

2. Tectonic Setting

At the Galapagos triple junction, the C-N Rift does not meet the EPR in a true Ridge-Ridge-Ridge configuration (Lonsdale, 1977, 1988; Schouten et al., 2008; Searle & Francheteau, 1986; Smith et al., 2011, 2013; Zonenshain

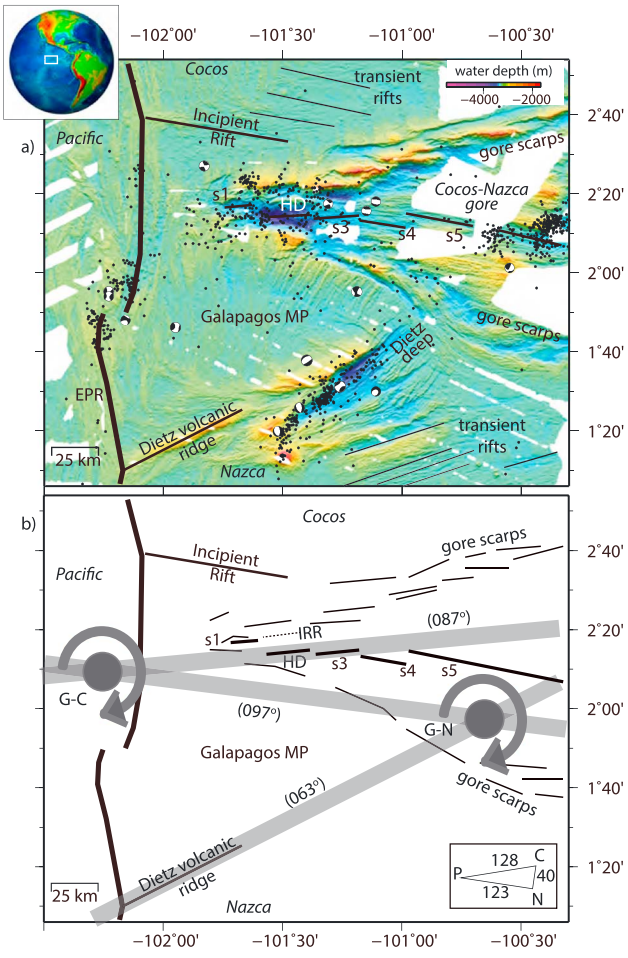

Figure 1. (a) Bathymetry of the western tip of the C-N Rift. Black dots: hydrophone-recorded earthquakes (Fox et al., 2001). Beach balls: focal mechanisms of teleseismically recorded earthquakes (Ekström et al., 2012). Thick black lines: plate boundaries. Thin black lines: area of transient rifts (Schouten et al., 2008; Smith et al., 2011). Rift segments labeled. HD: Hess Deep rift. EPR: East Pacific Rise. MP: microplate. Inset: study area in the equatorial eastern Pacific. (b) Diagram of the instantaneous relative rotation axes G-C and G-N. The velocity triangle shows motion of the major plates (NUVEL 1A; DeMets et al., 1994). P: Pacific; C: Cocos; N: Nazca; G: Galapagos. (097°) is a great circle passing through the faraway C-N axis and the locus of both the G-C and G-N axes (Schouten et al., 1993). (063°) runs along the strike of Dietz volcanic ridge, and (087°) runs along the strike of HD rift and segment s3 and is the locus of, respectively, the G-N and G-C axes assuming orthogonal spreading. A final requirement is that G-N velocity equals 40 mm/yr (C-N velocity) at the location of the G-C axis (i.e., at this point G does not move relative to C) and 33 mm/yr at Dietz volcanic ridge (Smith et al., 2011). This solution predicts an instantaneous angular velocity for Galapagos microplate of 12.7°/Myr relative to the major plates and a consequent total opening rate between Cocos and Galapagos at s1, HD rift, and s3 of ~16, ~19, and ~24 mm/yr, respectively. IRR: intrarift ridge.

et al., 1980); instead the Rift tip stops ~25 km east of the EPR axis (Figure 1). Two secondary rifts do link with the EPR forming true Ridge-Ridge-Ridge triple junctions. In the south at 1°10′N, Dietz volcanic ridge intersects the EPR and presently forms the southern boundary of the Galapagos microplate. To the north, Incipient Rift intersects the EPR at 2°40′N to form the northern triple junction (Klein et al., 2005; Lonsdale, 1988; Lonsdale et al., 1992; Schouten et al., 2008; Smith et al., 2011, 2013).

Schouten et al. (2008) identified a succession of older rifts northeast of Incipient Rift and concluded that Incipient Rift is just the latest of a sequence of southeast-trending cracks that jumped southwestward during the last 5 Ma, each accommodating some minor extension of EPR-generated crust (Figure 1a). The western tips of these cracks mark the trace of the northern triple junction. Schouten et al. (2008) explained the transient rifts using a crack interaction model, which would indicate that in the last 5 Ma the C-N Rift tip has remained at a variable distance to the EPR of 20–50 km. This model also predicts that cracking should be symmetric about the C-N Rift tip. Subsequently, Smith et al. (2011) documented a similar succession of transient rifts that formed southeast of the Galapagos microplate between 2.5 and 1.5 Ma. At ~1.4 Ma, however, extension became fixed on the last of the southern cracks and the Galapagos microplate developed (Smith et al., 2013).

3. Segments at the C-N Rift Tip

As the C-N Rift propagates westward, it produces a v-shaped section of seafloor bordered by the large, initial faults that cut the ~0.5 Ma EPR lithosphere (C-N gore; Holden and Dietz, 1972). We examine the sequence of rifts developing within the gore directly behind the Rift tip to characterize how full magmatic spreading is established at the C-N spreading center.

Searle and Francheteau (1986) noted an extensional rift basin (s1; Figures 1 and 2) located west of Hess Deep rift and offset ~2 km north. We interpret this 12-km-long basin as representing the earliest stage of rifting behind the Rift tip. Its current bounding faults will become the gore border scarps. The segment east of s1 is Hess Deep rift. It is ~25 km long and displays significant changes in morphology along its axis. A deep basin in the western half of the segment reaches water depths of 5,400 m and contains isolated areas of volcanic relief (Lonsdale, 1988). In the eastern half, more voluminous eruptions have built an axial volcanic ridge (AVR) ~11 km long and up to 500 m high (Figure 3a). From west to east along the AVR, water depths shallow from ~4,800 to ~4,100 m.

The next segment east, s3, is ~20 km long. A shallow graben containing small volcanic cones runs along the axis. This morphology is typical of spreading segments farther east on the C-N spreading center (Searle, 1989). The average water depth of s3 (~4,100 m) is just a few hundred meters deeper than that of s4.

Lonsdale (1977) and Searle and Francheteau (1986) suggested that seafloor spreading begins within Hess Deep rift. Based on its axial morphology, we interpret Hess Deep rift to be the transitional segment from rifting to spreading and suggest that full magmatic spreading is established first at segment s3. Hydroacoustically and teleseismically recorded earthquakes (Ekström et al., 2012; Fox et al., 2001) support this interpretation. From the C-N Rift tip to ~101°20′W, earthquakes (i.e., extension) are distributed over a cross-gore width of ~40 km encompassing the gore scarps and subsequent faults formed closer to

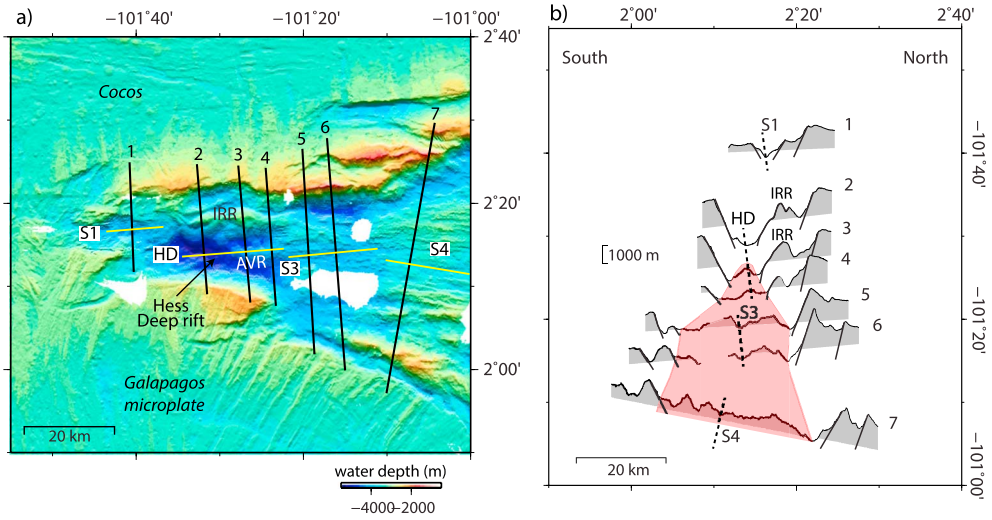

Figure 2. Bathymetry of C-N Rift. (a) Numbered black lines: location of bathymetric profiles in (b). Rift segments are labeled. HD: Hess Deep. AVR: axial volcanic ridge. IRR: intrarift ridge. (b) Bathymetric profiles along lines in (a). North to the right. Gray shading: sections <4,000 m deep. Faults are shown schematically subseafloor. Red shading: volcanic seafloor.

axis (Figure 1a). Beginning at segment s3, however, the number of earthquakes decreases significantly, suggesting that the gore scarps have been abandoned, and magmatic spreading has begun. Farther east, earthquakes are located primarily near the ridge axis likely associated with active normal faults, which commonly border intermediate-spreading ridges.

Both Hess Deep rift and s3 trend ~087° (s1 trend is poorly constrained), which suggests that they open within the Cocos-Galapagos microplate spreading regime (G-C, Figure 1b). Starting at ~101°10′W (segment s4) the ridge axis trends ~099°. This orientation is similar to the NUVEL 1A value of 097° for an orthogonal segment opening between Cocos and Nazca. If full magmatic seafloor spreading begins at s3, then the transition to spreading is occurring entirely within the Cocos-Galapagos microplate opening regime.

4. The Intrarift Ridge Within Hess Deep

Intrarift ridge (IRR) is located on the northern side of the Hess Deep rift and inward of the gore scarps (Figures 2 and 3). It extends ~20 km along the axis. Deep-seated rocks have been sampled from its top and slopes. The IRR has been studied for over two decades, and two expeditions (ODP Leg 147 and IODP Leg 345) drilled the IRR with the goal of understanding the structure and architecture of the lower crust and mantle exposed in this region (e.g., Francheteau et al., 1990; Gillis, Mevel, et al., 1993; Gillis et al., 2014; Hekinian et al., 1993; Karson et al., 2002; Lissenberg et al., 2013; Lonsdale, 1977; MacLeod et al., 1996; Rioux et al., 2012; Searle & Francheteau, 1986; Stewart et al., 2002, 2003).

The IRR has been interpreted by some as a south-facing, low-angle, long-lived normal fault (detachment fault; e.g., Ballu et al., 1999; Francheteau et al., 1990; Lonsdale, 1988; Wiggins et al., 1996). If IRR is a detachment fault, then we can speculate on magma supply to Hess Deep rift based on studies of oceanic detachment faults (e.g., Buck et al., 2005; Olive et al., 2010; Tucholke et al., 2008) and detachment faults at other rifted margins (e.g., Abers et al., 2016; Almalki et al., 2015, and references therein; Hill et al., 1995; Lavier & Manatschal, 2006).

Detachment faults have distinctive shapes. As a fault continues to slip, the footwall rolls over to near horizontal, domes upward, and is often corrugated. A narrow ridge commonly backs a detachment fault. And, because detachment faults are long-lived, they bring lower crust and upper mantle rocks to the seafloor.

A fault flexure model (Buck, 1988) with a constant effective elastic lithospheric thickness $Te = 0.5–1.0$ km successfully describes the domal shapes of the toes of a number of oceanic detachment faults in the central North Atlantic (Schouten et al., 2010). The flexure model also explains the linear ridge backing a detachment fault. This ridge is the breakaway of a rotated normal fault, and the outward-facing slopes of the ridge are back-tilted sections of originally subhorizontal median valley floor (MacLeod et al., 2009; Smith et al.,

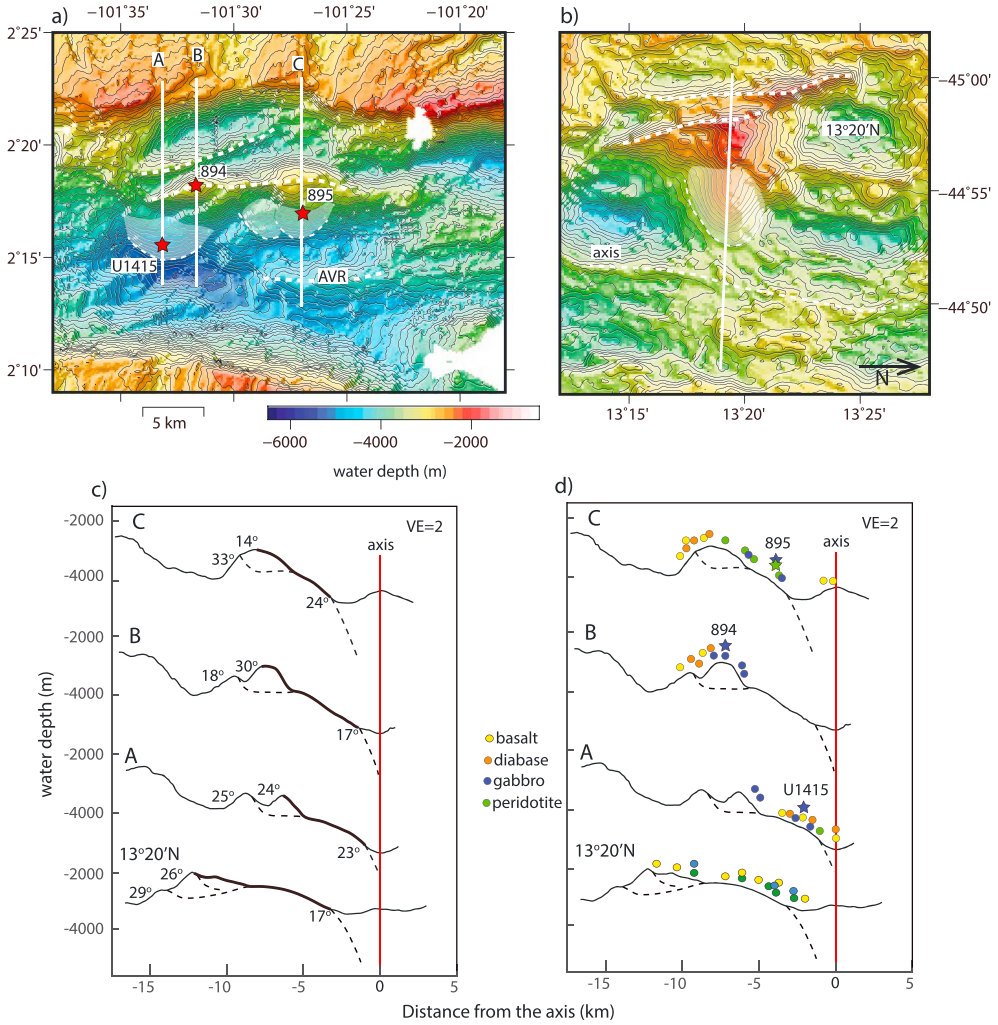

Figure 3. Bathymetry of (a) intrarift ridge and (b) 13°20′N detachment at the Mid-Atlantic Ridge (north is to the right). Contour interval: 100 m. Red stars: ODP and IODP drill sites (e.g., Francheteau et al., 1990; Gillis et al., 2014; Gillis, Thompson, et al., 1993; Tominaga et al., 2016). Thick white lines: locations of profiles in (c). Shaded region: toes of the IRR and 13°20′N detachment faults. Thin dashed lines: outlines of terminations. Dashed white lines: rift axis and possible fault breakaways. (c) Profiles along lines shown in (a) and (b). The IRR profiles were chosen to cross close to the ODP/IODP drill sites. Thick black lines: exposed detachment footwall. Dashed black lines: faults shown schematically subsurface assuming flexural rotation. Fault dips indicated. (d) Colored circles: rocks sampled near profiles. Colored stars: rocks recovered by drilling.

2008). To evaluate whether IRR might be a detachment fault, we compare its shape to a well-studied, active detachment fault at the slow spreading (25 mm/yr) Mid-Atlantic Ridge (MAR) at 13°20′N. The 13°20′N fault displays the characteristics common to many long-lived flexurally rotated oceanic detachment faults (e.g., Bonnemains et al., 2017; Escartín et al., 2017; MacLeod et al., 2009; Mallows & Searle, 2012; Parnell-Turner et al., 2017; Smith et al., 2008, 2006).

Even though the MAR and Hess Deep rift represent two very different settings we still think that a comparison of these two features is meaningful. The IRR fault is forming inward of the large, mostly unrotated faults that initially cut the 0.5 Ma lithosphere and accommodated extension between Cocos and Galapagos microplate. Because the IRR fault appears to root beneath the axis, as does the 13°20′N detachment fault, we consider IRR part of the developing spreading regime. Volcanism at the axis of both the MAR in the 13°N region and Hess Deep rift indicate that magma is present beneath the rifts, which reduces plate strength (commonly expressed as the effective elastic thickness of the plate, *Te*). Based on the shape of the toe of the active 13°20′N detachment and other MAR detachment faults, *Te* is estimated to be 0.5–1.0 km (Schouten et al., 2010). The shape of the toe of the IRR fault yields a similar value for *Te* (1–2 km).

The IRR and the 13°20′N detachment are plotted at the same scale in Figures 3a and 3b. Bathymetric profiles are shown in Figure 3c, and rock lithologies sampled near the profile locations are shown schematically above the profiles in Figure 3d (e.g., Francheteau et al., 1990; Gillis et al., 2014; Gillis, Thompson, et al., 1993; Rioux et al., 2012; Tominaga et al., 2016).

The 13°20′N detachment extends ~10 km along the axis. Its termination is curved, and a domed and corrugated footwall emerges from beneath the valley floor along the termination. The corrugated surface dips at ~17° where it emerges and gradually rolls over to near horizontal as it continues to slip. Jumbled-looking terrain borders the western edge of the corrugations, and west of that, two narrow ridges back the detachment fault. Basalt, gabbro, and peridotite were sampled from the 13°20′N footwall (Escartín et al., 2017).

The bathymetry of the IRR is not as simple as that of the 13°20′N detachment. The IRR extends along the axis for ~20 km and appears to be a composite of at least two domed detachments with curved terminations (Figure 3a). This is not unusual; compound detachment faults have been described in the 13°N region (Cannat et al., 2013; Smith et al., 2008). The dip of the footwall of the IRR where it emerges ranges between ~17° and 24° on the profiles shown (Figure 3c). Gabbro and peridotites were sampled from the top and southern slopes of the IRR (Figure 3d). Dredging on the northern slope yielded mainly basalt and dolerite, although gabbro was obtained near Line B. Dredges from the narrow ridge 2 km north of the IRR western section yielded mainly basalt and dolerite.

We use the fault flexure model to help interpret the fault geometry along the bathymetric profiles (Figure 3c). The solid black lines mark the interpreted exposed footwall of the detachments. Deciphering the subsurface geometry of detachment faults is more complicated because they may be covered by rafted blocks which are slices of hanging wall cut off by normal faults that root in the same primary fault (Buck & Poliakov, 1998; Reston & Ranero, 2011; Smith et al., 2008). Therefore, a fault could bound a rafted block or it could be a separate new fault. As an example, the narrow ridge north of IRR might be the IRR fault breakaway. This would imply that the distinctive high of the IRR is a rafted block (Figure 3c). Alternatively, the breakaway could be at the top of the IRR. If rafted blocks are present, their compositions would likely be different in the two settings because the 13°20′N detachment borders a mature spreading center while IRR borders an incipient spreading center. In Figure 3c, the subsurface shapes of the faults are shown for some of the possible interpretations (dashed lines drawn by hand).

Using the interpretations shown in Figure 3c we estimate a number of fault parameters. Fault heave is the horizontal distance between the fault breakaway and the termination. At the 13°20′N detachment, the heave is ~9 or 11 km, depending on the interpretation of the breakaway. Estimates of heave for IRR are in a similar range. The heave on Line A is ~6 or 8 km, Line B is ~6 or 11 km, and Line C is ~5 or 6 km.

We also compare the back-tilts of the possible breakaway ridges. At the 13°20′N back-tilts of ~26° and ~29° were obtained for the two ridges (Figure 3b) from near-bottom, high-resolution bathymetry data (MacLeod et al., 2009). Corresponding inward-facing dips are 25° and 15°. Summing the two dips together gives initial fault dips of 51° and 44°. At the IRR, back-tilts of possible breakaway ridges were obtained from lower-resolution multibeam bathymetry data and range between 14° and 33°. Corresponding inward-facing dips of the ridges fall between 16° and 36° yielding initial fault dips between 35° and 66°. These values are comparable to those reported by MacLeod et al. (2009) for rotated fault blocks in the 13°N region.

The shape of the detachment footwall as it emerges at the termination is a key diagnostic for recognizing long-lived detachment faults. As mentioned above, the dip of the footwall of the 13°20′N detachment where it emerges is ~17°, and the dip of the IRR footwall ranges between 17° and 24°. Assuming an initial fault dip of 60°, these values indicate significant flexural rotation of the fault. Both the footwall of the 13°20′N detachment and the IRR roll over to near horizontal within ~3–4 km of the termination.

High-resolution near-bottom bathymetry data collected near the toe of the IRR (western shaded region, Figure 3a; Ferrini et al., 2013) and the 13°20′N detachment (Escartín et al., 2017) show fault toes with similar shapes. Both footwalls are convex upward with a width of ~4 km and an apex 400–500 m above neighboring seafloor.

We acknowledge that mass wasting could alter the shape of the detachment footwall significantly, and considerable mass wasting has been suggested at the IRR (Ferrini et al., 2013). The similarity in the bathymetric profiles across the IRR and 13°20′N, however, suggests that mass wasting may only be surficial as suggested more recently by Tominaga et al. (2016).

Based on the overall shape of the IRR and its similarity to the 13°20′N detachment, we propose it is a flexurally rotated, long-lived detachment fault. Paleomagnetic data from the top of IRR (ODP site 894) indicate >40° of northward rotation about a moderately eastward plunging axis (MacLeod et al., 1996). Although the value is high, it is consistent with a flexurally rotated fault model.

One notable difference between IRR and 13°20′N is that the 13°20′N footwall is corrugated over several spatial scales. In contrast, the IRR lacks observable corrugations at any scale. It may be that mass wasting has been sufficient to mask corrugations, which typically have amplitudes of tens of meters on the multibeam bathymetry (Smith et al., 2014). It also is possible that significant corrugations do not always form on long-lived faults. The implications of IRR being a detachment fault are discussed below.

5. Discussion

The Galapagos triple junction region provides an opportunity to examine the transition from rifting of oceanic lithosphere to seafloor spreading. This transition occurs along Hess Deep rift, where we suggest that spreading and detachment faulting are occurring. Magmatic spreading is fully established at the adjacent segment (s3), which is morphologically similar to magmatic spreading segments farther east along the C-N Rift (shallow graben with small volcanoes; Searle, 1989). The distribution of seismicity indicates that extension is accommodated on both the gore faults and the rift axis faults bordering segments s1 and Hess Deep rift. This is not the case for segment s3. Seismicity decreases sharply at segment s3. At rifted margins elsewhere, it has been suggested that once sufficient magma is present in the rift system, it will weaken the lithosphere and help localize deformation along the newly formed rift axis (e.g., Woodlark Basin, Taylor et al., 1999; East African Rift, Ebinger & Casey, 2001). Thus, the cessation of widespread seismicity near the eastern end of Hess Deep rift supports the idea that full magmatic spreading begins at s3, with magmatism accommodating most of the extension.

The IRR is located within Hess Deep rift and within the broad zone of seismicity. The similarity of its shape to that of the active 13°20′N detachment fault at the MAR, and the exposure of lower crust and upper mantle rocks on its top and flanks, leads us to conclude that it is a low-angle detachment fault; the associated seismicity suggests that it is active.

Low-angle detachments are observed at Woodlark basin where they are active before the onset of seafloor spreading (Taylor et al., 1999), and studies there have proposed that detachment fault formation signals the input of magma into the area (e.g., Hill et al., 1995; Little et al., 2007; Martinez et al., 2001; Taylor et al., 1999). Studies of oceanic detachment faults along slower spreading ridges also suggest that magma supply plays an important role in the initiation and maintenance of slip on long-lived detachment faults (Whitney et al., 2013, and references therein). It has been suggested that there is a threshold of melt supply above and below which oceanic detachment faults do not form (e.g., Buck et al., 2005; Olive et al., 2010; Tucholke et al., 2008). If this is the case, then magma supply to Hess Deep rift must fall within the range necessary for oceanic detachment fault formation.

There is evidence of magmatism at the Hess Deep rift axis. Volcanic relief has been described within the deep rift in the western half (Lonsdale, 1988), and a fully developed AVR has been built in the eastern half of the segment. Such diversity in the expression of volcanism in the presence of detachment faults is not unusual: Active detachment faults are found bordering MAR rift valleys containing large AVRs (Smith et al., 2014) as well as rift valleys with little evidence of seafloor volcanism (Smith et al., 2014; Tucholke et al., 1998).

An interesting question is whether detachment fault formation represents a common stage in the transition from rifting to seafloor spreading behind the C-N Rift tip. An inspection of the available data inward of the gore scarps (Figure 1) out to about ~101°W (~5 Ma of C-N Rift propagation) yields no feature similar to the IRR. From the presumed absence of other detachments, we conclude that the normal mode of C-N Rift propagation has not favored detachment fault formation during the transition to magmatic spreading.

A possible explanation is that IRR is a manifestation of a slowdown in spreading rate, and presumed decrease in magma supply, associated with the formation of the Galapagos microplate (~1.4 Ma). Before 1.4 Ma, opening was between Cocos and Nazca at an intermediate spreading rate of ~40 mm/yr all the way to the C-N Rift tip. Segments s1, Hess Deep rift, and s3, however, are part of a new

plate kinematic system. These segments open between Cocos and the Galapagos microplate at the very slow spreading rates of ~16, ~19, and ~24 mm/yr, respectively (spreading rate estimates based on the diagram of instantaneous relative rotation axes G-C and G-N in Figure 1b).

It is difficult to explain, however, why no detachment borders s3, which is also opening within the Cocos-Galapagos microplate spreading regime. Hess Deep rift may be the first segment that has responded to the slowdown in opening rate and associated change in magma supply. The formation of the IRR detachment at a spreading rate of 19 mm/yr is consistent with the very slow spreading rates associated with the exhumation of mantle in Woodlark Basin (Benes et al., 1994), the Southwest Indian Ridge (e.g., Cannat et al., 2006), and the magma-poor rifted margins in the North Atlantic (e.g., Reston & McDermott, 2011; Sibuet et al., 2007).

When will full magmatic spreading be established at Hess Deep rift? Segment s3 is spreading magmatically, and its western end is currently ~50 km from the C-N Rift tip. The western end of Hess Deep rift is ~25 km from the Rift tip. The C-N rift propagates westward at roughly half the EPR spreading rate (64 mm/yr), and if the transition propagates at the same rate, Hess Deep rift will be spreading magmatically in $<$0.5 Ma and s1 will become the new transition segment.

Since the present kinematics have not gone on for long, it will be necessary for more rift segments to form within the slow spreading regime between Cocos and Galapagos microplate to determine if detachment fault formation has become a phase in the transition to magmatic spreading. One consequence of IRR being a low-angle detachment fault, with melt supply to the axis, is that the IRR detachment fault may be exhuming gabbros emplaced beneath the Hess Deep Rift rather than at the EPR.

6. Summary

The sequence of developing spreading segments within in the wake of the westward propagating C-N Rift tip shows the transition from rifting to magmatic seafloor spreading. A 12-km-long basin (s1) represents the earliest stage of rifting. The 25-km-long Hess Deep rift is a transitional segment, and full magmatic spreading begins at the next segment (s3). The characteristics of the IRR located within Hess Deep Rift are compared to those of a well known, active oceanic detachment fault that is representative for detachments in the central North Atlantic. Based on this comparison, we conclude that IRR is also a long-lived detachment fault exhuming lower crust and upper mantle to the seafloor. Although transitional phases must have occurred throughout the propagation of the C-N Rift, IRR is the only obvious detachment fault along the edges of the gore in the last 5 Ma. IRR formation may be in response to a significant decrease in spreading rate (~40 to $<$20 mm/yr), caused by the formation of the Galapagos microplate ~1.4 Ma, which now controls the opening at the C-N Rift tip. Additional segments created by the propagation of the C-N Rift are needed before it will be possible to definitively assess the probability of the continued formation of detachment faults and any association with the local slow-down in spreading rates.

Acknowledgments

Multibeam bathymetry data are available from the Marine Geoscience Data System Web site (http://www.marine-geo.org/portals/ridge2000/); see Smith (2011). Hydrophone data are available from http://www.pmel.noaa.gov/acoustics/. Teleseismically recorded earthquakes are available from the Centroid Moment Tensor catalog (http://www.globalcmt.org/CMTsearch.html). Bathymetry data are displayed using Generic Mapping Tools software (Wessel & Smith, 1991). D.K.S. and H.S were supported in part by WHOI. We had helpful discussions with M. Cannat, S. Carbotte, K. Gillis, E. Klein, and B. Tucholke. Any opinion, findings, and conclusions or recommendations expressed in this material are those of the authors and do not necessarily reflect the views of the National Science Foundation.

References

Abers, G. A., Eilon, Z., Gaherty, J. B., Jin, G., Kim, Y. H., Obrebski, M., & Dieck, C. (2016). Southeast Papuan crustal tectonics: Imaging extension and buoyancy of an active rift. *Journal of Geophysical Research: Solid Earth*, *121*, 951–971. https://doi.org/10.1002/2015JB012621

Almalki, K. A., Betts, P. G., & Ailleres, L. (2015). The Red Sea—50 years of geological and geophysical research. *Earth-Science Reviews*, *147*, 109–140. https://doi.org/10.1016/j.earscirev.2015.05.002

Augustin, N., Devey, C. W., van der Zwan, F. M., Feldens, P., Tominaga, M., Bantan, R. A., & Kwasnitschka, T. (2014). The rifting to spreading transition in the Red Sea. *Earth and Planetary Science Letters*, *395*, 217–230. https://doi.org/10.1016/j.epsl.2014.03.047

Ballu, V., Hildebrand, J. A., & Canuteson, E. L. (1999). The density structure associated with oceanic crustal rifting at the Hess Deep: A seafloor and sea-surface gravity study. *Earth and Planetary Science Letters*, *171*(1), 21–34. https://doi.org/10.1016/S0012-821X(99)00132-6

Bastow, I. D., Pilidou, S., Kendall, J. M., & Stuart, G. W. (2010). Melt-induced seismic anisotropy and magma assisted rifting in Ethiopia: Evidence from surface waves. *Geochemistry, Geophysics, Geosystems*, *11*, Q0AB05. https://doi.org/10.1029/2010GC003036

Benes, V., Scott, S. D., & Binns, R. A. (1994). Tectonics of rift propagation into a continental margin: Western Woodlark Basin, Papua New Guinea. *Journal of Geophysical Research*, *99*(B3), 4439–4455. https://doi.org/10.1029/93JB02878

Bonatti, E. (1985). Punctiform initiation of seafloor spreading in the Red Sea during transition from a continental to an oceanic rift. *Nature*, *316*(6023), 33–37. https://doi.org/10.1038/316033a0

Bonnemains, D., Escartín, J., Mével, C., Andreani, M., & Verlaguet, A. (2017). Pervasive silicification and hanging wall overplating along the 13°20′N oceanic detachment fault (Mid-Atlantic Ridge). *Geochemistry, Geophysics, Geosystems*, *18*, 2028–2053. https://doi.org/10.1002/2017GC006846

Buck, W. R. (1988). Flexural rotation of normal faults. *Tectonics*, *7*(5), 959–973. https://doi.org/10.1029/TC007i005p00959

Buck, W. R., Lavier, L. L., & Poliakov, A. N. B. (2005). Modes of faulting at mid-ocean ridges. *Nature*, *434*(7034), 719–723. https://doi.org/10.1038/nature03358

Buck, W. R., & Poliakov, A. N. B. (1998). Abyssal hills formed by stretching oceanic lithosphere. *Nature*, *392*(6673), 272–275. https://doi.org/10.1038/32636

Cannat, M., Mangeney, A., Ondréas, H., Fouquet, Y., & Normand, A. (2013). High-resolution bathymetry reveals contrasting landslide activity shaping the walls of the Mid-Atlantic Ridge axial valley. *Geochemistry, Geophysics, Geosystems*, *14*(4), 996–1011. https://doi.org/10.1002/ggge.20056

Cannat, M., Sauter, D., Mendel, V., Ruellan, E., Okino, K., Escartin, J., et al. (2006). Modes of seafloor generation at a melt-poor ultraslow-spreading ridge. *Geology*, *34*(7), 605–608. https://doi.org/10.1130/G22486.1

DeMets, C., Gordon, R. G., Argus, D. F., & Stein, S. (1994). Effect of recent revisions to the geomagnetic reversal time scale on estimates of current plate motions. *Geophysical Research Letters*, *21*(20), 2191–2194. https://doi.org/10.1029/94GL02118

Ebinger, C., & Casey, M. (2001). Continental breakup in magmatic provinces: An Ethiopian example. *Geology*, *29*(6), 527–530. https://doi.org/10.1130/0091-7613(2001)029<0527:CBIMPA>2.0.CO;2

Ekström, G., Nettles, M., & Dziewonski, A. M. (2012). The global CMT project 2004–2010: Centroid-Moment Tensors for 13,017 earthquakes. *Physics of the Earth and Planetary Interiors*, *200-201*, 1–9. https://doi.org/10.1016/j.pepi.2012.1004.1002

Escartín, J., Mével, C., Petersen, S., Bonnemains, D., Cannat, M., Andreani, M., et al. (2017). Tectonic structure, evolution, and the nature of oceanic core complexes and their detachment fault zones (13°20′N and 13°30′N, Mid-Atlantic Ridge). *Geochemistry, Geophysics, Geosystems*, *18*, 1451–1482. https://doi.org/10.1002/2016GC006775

Ferrini, V. L., Shillington, D. J., Gillis, K., MacLeod, C. J., Teagle, D. A. H., Morris, A., et al. (2013). Evidence of mass failure in the Hess Deep Rift from multi-resolutional bathymetry data. *Marine Geology*, *339*, 13–21. www.sciencedirect.com/science/article/pii/S0025322713000364

Fox, C. G., Matsumoto, H., & Lau, T.-K. (2001). Monitoring Pacific Ocean seismicity from an Autonomous Hydrophone Array. *Journal of Geophysical Research*, *106*(B3), 4183–4206. https://doi.org/10.1029/2000JB900404

Francheteau, J., Armijo, R., Cheminee, J. L., Hekinian, R., Lonsdale, P., & Blum, N. (1990). 1 Ma East Pacific Rise oceanic crust and uppermost mantle exposed by rifting in Hess Deep (equatorial Pacific Ocean). *Earth and Planetary Science Letters*, *101*(2-4), 281–295. https://doi.org/10.1016/0012-821X(90)90160-Y

Gillis, K. M., Mevel, C., & Allan, J. F. (1993). *Proc. ODP, Init. Repts.* (Vol. 147). College Station, TX: Ocean Drilling Program. https://doi.org/10.2973/odp.proc.ir.2147.1993

Gillis, K. M., Snow, J. E., Klaus, A., Abe, N., Adriao, A. B., Akizawa, N., et al. (2014). Primitive layered gabbros from fast-spreading lower oceanic crust. *Nature*, *505*(7482), 204–207. https://doi.org/10.1038/nature12778

Gillis, K. M., Thompson, G., & Kelley, D. S. (1993). A view of the lower crustal component of hydrothermal systems at the Mid-Atlantic Ridge. *Journal of Geophysical Research*, *98*(B11), 19,597–19,619. https://doi.org/10.1029/93JB01717

Hayward, N. J., & Ebinger, C. J. (1996). Variations in the along-axis segmentation of the Afar Rift system. *Tectonics*, *15*(2), 244–257. https://doi.org/10.1029/95TC02292

Hekinian, R., Bideau, D., Francheteau, J., Cheminee, J. L., Armijo, R., Lonsdale, P., & Blum, N. (1993). Petrology of the East Pacific Rise crust and upper mantle exposed in Hess Deep (eastern equatorial Pacific). *Journal of Geophysical Research*, *98*(B5), 8069–8094. https://doi.org/10.1029/92JB02072

Hill, E. J., Baldwin, S. L., & Lister, G. S. (1995). Magmatism as an essential driving force for formation of active metamorphic core complexes in eastern Papua New Guinea. *Journal of Geophysical Research*, *100*(B6), 10,441–10,451. https://doi.org/10.1029/94JB03329

Holden, J. C., & Dietz, R. S. (1972). Galapagos Gore, NazCoPac Triple Junction and Carnegie/Cocos ridges. *Nature*, *235*(5336), 266–269. https://doi.org/10.1038/235266a0

Karson, J. A., Klein, E. M., Hurst, S. D., Lee, C. D., Rivizzigno, P. A., Curewitz, D., et al. (2002). Structure of uppermost fast-spreading oceanic crust exposed at the Hess Deep Rift: Implications for subaxial processes at the East Pacific Rise. *Geochemistry, Geophysics, Geosystems*, *3*, 1002. https://doi.org/10.1029/2001GC000155

Klein, E. M., Smith, D. K., Williams, C. M., & Schouten, H. (2005). Counter-rotating microplates at the Galapagos Triple Junction, eastern equatorial Pacific Ocean. *Nature*, *433*(7028), 855–858. https://doi.org/10.1038/nature03262

Lavier, L. L., & Manatschal, G. (2006). A mechanism to thin the continental lithosphere at magma-poor margins. *Nature*, *440*(7082), 324–328. https://doi.org/10.1038/nature04608

Ligi, M., Bonatti, E., Bortoluzzi, G., Cipriani, A., Cocchi, L., Caratori Tontini, F., et al. (2012). Birth of an ocean in the Red Sea: Initial pangs. *Geochemistry, Geophysics, Geosystems*, *13*, Q08009. https://doi.org/10.1029/02012GC004155

Lissenberg, C. J., MacLeod, C. J., Howard, K. A., & Godard, M. (2013). Pervasive reactive melt migration through fast-spreading lower oceanic crust (Hess Deep, equatorial Pacific Ocean). *Earth and Planetary Science Letters*, *361*, 436–447. https://doi.org/10.1016/j.epsl.2012.11.012

Little, T. A., Baldwin, S. L., Fitzgerald, P. G., & Monteleone, B. (2007). Continental rifting and metamorphic core complex formation ahead of the Woodlark spreading ridge, D'Entrecasteaux Islands, Papua New Guinea. *Tectonics*, *26*, TC1002. https://doi.org/10.1029/2005TC001911

Lonsdale, P. (1977). Regional shape and tectonics of the equatorial East Pacific Rise. *Marine Geophysical Researches*, *3*(3), 295–315. https://doi.org/10.1007/BF00285657

Lonsdale, P. (1988). Structural patterns of the Galapagos microplate and evolution of the Galapagos Triple Junction. *Journal of Geophysical Research*, *93*(B11), 13,551–13,574. https://doi.org/10.1029/JB093iB11p13551

Lonsdale, P. (1989). Geology and tectonic history of the Gulf of California. In E. L. Winterer, D. M. Hussong, & R. W. Decker (Eds.), *The geology of North America, the eastern Pacific Ocean and Hawaii* (Vol. N, pp. 499–521). Boulder, CO: Geological Society of America.

Lonsdale, P., Blum, N., & Puchelt, H. (1992). The RRR triple junction at the southern end of the Pacific-Cocos East Pacific Rise. *Earth and Planetary Science Letters*, *109*(1-2), 73–85. https://doi.org/10.1016/0012-821X(92)90075-7

MacLeod, C. J., Früh-Green, G. L., & Manning, C. E. (1996). Tectonics of Hess Deep: A synthesis of drilling results from leg 147. In C. Mével, K. M. Gillis, J. F. Allan, & P. S. Meyer (Eds.), *Proc. of the Ocean Drilling Program, Sci. Res.* (Vol. 147, pp. 461–475). College Station, TX: Ocean Drilling Program.

MacLeod, C. J., Searle, R. C., Murton, B. J., Casey, J. F., Mallows, C., Unsworth, S. C., et al. (2009). Life cycle of oceanic core complexes. *Earth and Planetary Science Letters*, *287*(3-4), 333–344. https://doi.org/10.1016/j.epsl.2009.08.016

Mallows, C., & Searle, R. C. (2012). A geophysical study of oceanic core complexes and surrounding terrain, Mid-Atlantic Ridge 13°N–14°N. *Geochemistry, Geophysics, Geosystems*, *13*, Q0AG08. https://doi.org/10.1029/2012GC004075

Manighetti, I., Tapponier, P., Courtillot, V., Gruszow, S., & Gillot, P.-Y. (1997). Propagation of rifting along the Arabia-Somalia plate boundary: The Gulfs of Aden and Tadjoura. *Journal of Geophysical Research*, *102*(B2), 2681–2710. https://doi.org/10.1029/96JB01185

Martinez, F., & Cochran, J. R. (1988). Structure and tectonics of the northern Red Sea: Catching a continental margin between rifting and drifting. *Tectonophysics*, *150*(1-2), 1–31. https://doi.org/10.1016/0040-1951(88)90293-4

Martinez, F., Goodliffe, A. M., & Taylor, B. (2001). Metamorphic core complex formation by density inversion and lower-crust extrusion. *Nature*, *411*, 911–932.
Olive, J.-A., Behn, M. D., & Tucholke, B. E. (2010). The structure of oceanic core complexes controlled by the depth distribution of magma emplacement. *Nature Geoscience*, *6*(9), 755–760. https://doi.org/10.1038/NGEO1888
Parnell-Turner, R. E., Sohn, R. A., Peirce, C., Reston, T. J., MacLeod, C. J., Searle, R. C., & Simao, N. M. (2017). Oceanic detachment faults generate compression in extension. *Geology*, *45*(10), 923–926. https://doi.org/10.1130/G39232.1
Reston, T. J., & McDermott, K. G. (2011). Successive detachment faults and mantle unroofing at magma-poor rifted margins. *Geology*, *39*(11), 1071–1074. https://doi.org/10.1130/G32428.1
Reston, T. J., & Ranero, C. R. (2011). The 3-D geometry of detachment faulting at mid-ocean ridges. *Geochemistry, Geophysics, Geosystems*, *12*, Q0AG05. https://doi.org/10.1029/2011GC003666
Rioux, M., Johan Lissenberg, C., McLean, N. M., Bowring, S. A., MacLeod, C. J., Hellebrand, E., & Shimizu, N. (2012). Protracted timescales of lower crustal growth at the fast-spreading East Pacific Rise. *Nature Geoscience*, *5*(4), 275–278. https://doi.org/10.1038/ngeo1378
Rosendahl, B. R. (1987). Architecture of continental rifts with special reference to East Africa. *Annual Review of Earth and Planetary Sciences*, *15*(1), 445–503. https://doi.org/10.1146/annurev.ea.15.050187.002305
Schouten, H., Klitgord, K. D., & Gallo, D. G. (1993). Edge-driven microplate kinematics. *Journal of Geophysical Research*, *98*(B4), 6689–6701. https://doi.org/10.1029/92JB02749
Schouten, H., Smith, D. K., Cann, J. R., & Escartin, J. (2010). Tectonic versus magmatic extension in the presence of core complexes at slow-spreading ridges from a visualization of faulted seafloor topography. *Geology*, *38*, 615–618. https://doi.org/10.1130/G30803.1
Schouten, H., Smith, D. K., Montési, L., Zhu, W., & Klein, E. M. (2008). Unstable northern rifts of the Galapagos Triple Junction, Eastern Equatorial Pacific. *Geology*, 330–342. https://doi.org/10.1130/G24431A.1
Searle, R. C. (1989). Location and segmentation of the Cocos-Nazca Spreading Centre west of 95°W. *Marine Geophysical Researches*, *11*(1), 15–26. https://doi.org/10.1007/BF00286245
Searle, R. C., & Francheteau, J. (1986). Morphology and tectonics of the Galapagos Triple Junction. *Marine Geophysical Researches*, *8*, 95–129.
Sibuet, J.-C., Srivastava, S., & Manatschal, G. (2007). Exhumed mantle-forming transitional crust in the Newfoundland-Iberia rift and associated magnetic anomalies. *Journal of Geophysical Research*, *112*, B06105. https://doi.org/10.1029/2005JB003856
Smith, D. K. (2011). *Grid(S) of multibeam bathymetry at Galapagos Triple Junction*. Palisades, New York: Integr. Earth Data Appl. https://doi.org/10.1594/IEDA/100005
Smith, D. K., Cann, J. R., & Escartin, J. (2006). Widespread active detachment faulting and core complex formation near 13°N on the Mid-Atlantic Ridge. *Nature*, *442*(7101), 440–443. https://doi.org/10.1038/nature04950
Smith, D. K., Escartin, J., Schouten, H., & Cann, J. R. (2008). Fault rotation and core complex formation: Significant processes in seafloor formation at slow-spreading mid-ocean ridges (Mid-Atlantic Ridge, 13–25°N). *Geochemistry, Geophysics, Geosystems*, *9*, Q03003. https://doi.org/10.1029/02007GC001699
Smith, D. K., Schouten, H., Dick, H. J. B., Cann, J. R., Salters, V., Marschall, H. R., et al. (2014). Development and evolution of detachment faulting along 50 km of the Mid-Atlantic Ridge near 16.5°N. *Geochemistry, Geophysics, Geosystems*, *15*, 4692–4711. https://doi.org/10.1002/2014GC005563
Smith, D. K., Schouten, H., Montési, L., & Zhu, W. (2013). The recent history of the Galapagos Triple Junction preserved on the Pacific plate. *Earth and Planetary Science Letters*, *371-372*, 6–15. https://doi.org/10.1016/j.epsl.2013.1004.1018
Smith, D. K., Schouten, H., Zhu, W., Montési, L., & Cann, J. R. (2011). Distributed deformation ahead of the Cocos-Nazca Rift at the Galapagos Triple Junction. *Geochemistry, Geophysics, Geosystems*, *12*, Q11003. https://doi.org/10.1029/2011GC003689
Stewart, M. A., Klein, E. M., & Karson, J. A. (2002). The geochemistry of dikes and lavas from the North Wall of the Hess Deep Rift: Insights into the four-dimensional character of crustal construction at fast-spreading mid-ocean ridges. *Journal of Geophysical Research*, *107*(B10), 2238. https://doi.org/10.1029/2001JB000545
Stewart, M. A., Klein, E. M., Karson, J. A., & Brophy, J. A. (2003). Geochemical relationships between dikes and lavas at the Hess Deep Rift: Implications for magma eruptibility. *Journal of Geophysical Research*, *108*(B4), 2184. https://doi.org/10.1029/2001JB001622
Taylor, B., Goodliffe, A. M., & Martinez, F. (1999). How continents break up: Insights from Papua New Guinea. *Journal of Geophysical Research*, *104*(B4), 7497–7512. https://doi.org/10.1029/1998JB900115
Taylor, B., Goodliffe, A. M., Martinez, F., & Hey, R. N. (1995). Continental rifting and initial sea-floor spreading in the Woodlark basin. *Nature*, *374*(6522), 534–537. https://doi.org/10.1038/374534a0
Tominaga, M., Tivey, M. A., MacLeod, C. J., Morris, A., Lissenberg, C. J., Shillington, D. J., & Ferrini, V. (2016). Characterization of the in situ magnetic architecture of oceanic crust (Hess Deep) using near-source vector magnetic data. *Journal of Geophysical Research: Solid Earth*, *121*, 4130–4146. https://doi.org/10.1002/2015JB012783
Tucholke, B. E., Behn, M. D., Buck, W. R., & Lin, J. (2008). Role of melt supply in oceanic detachment faulting and formation of megamullions. *Geology*, *36*(6), 455–458. https://doi.org/10.1130/G24639A.24631
Tucholke, B. E., Lin, J., & Kleinrock, M. C. (1998). Megamullions and mullion structure defining oceanic metamorphic core complexes on the Mid-Atlantic Ridge. *Journal of Geophysical Research*, *103*(B5), 9857–9866. https://doi.org/10.1029/98JB00167
Van Wijk, J. W., & Blackman, D. K. (2005). Dynamics of continental rift propagation: The end-member modes. *Earth and Planetary Science Letters*, *229*(3–4), 247–258. https://doi.org/10.1016/j.epsl.2004.10.039
Wessel, P., & Smith, W. H. F. (1991). Free software helps map and display data. *Eos, Transactions of the American Geophysical Union*, *72*(41), 441. https://doi.org/10.1029/90EO00319
Whitney, D. L., Teyssier, C., Rey, P., & Buck, W. R. (2013). Continental and oceanic core complexes. *Geological Society of America Bulletin*, *125*(3–4), 273–298. https://doi.org/10.1130/B30754.1
Wiggins, S. M., Dorman, L. M., Cornuelle, B. D., & Hildebrand, J. A. (1996). Hess Deep Rift valley structure from seismic tomography. *Journal of Geophysical Research*, *101*(B10), 22,335–22,353. https://doi.org/10.1029/96JB01230
Zonenshain, L. P., Kogan, L. I., Savostin, L. A., Golmstock, A. J., & Gorodnitskii, A. M. (1980). Tectonics, crustal structure and evolution of the Galapagos Triple Junction. *Marine Geology*, *37*(3–4), 209–230. https://doi.org/10.1016/0025-3227(80)90102-4